JOURNAL OF MATERIALS SCIENCE 8 (1973) 41–46

Lamellar and interlamellar structure in melt-crystallized polyethylene

Part 3 *Effects of small deformation*

W. E. KAUFMAN*, J. M. SCHULTZ
Department of Chemical Engineering, University of Delaware, Newark, Delaware, USA

The effects of small (<20%) strain on the microstructure of Marlex 6009 polyethylene was investigated *in situ* by absolute small and wide-angle X-ray diffraction. The methods of analysis given in previous papers by Kavesh and Schultz were utilized. The degree of crystallinity decreased monotonically with strain. The "amorphous" density increased with strain to some 8 to 12% strain, after which the density levelled off at a value of about 0.901. The lamellar thickness was found to decrease slightly with strain while the intervening layer thickness increased. Finally, the plane of the carbon backbone rotated toward the *a-c* crystallographic plane as the strain increased. The microstructural effects are interpreted in the light of molecular rearrangements in both crystalline and "amorphous" zones.

1. Introduction

Previous papers in this series demonstrated the utility of absolute X-ray diffraction measurements in characterizing semicrystalline polyethylene [1, 2]. More specifically, the information obtainable is as follows.

(a) From "wide-angle" peak positions: unit cell parameters and the density of the crystalline phase.

(b) From absolute "wide-angle" line breadths: (1) crystallite size, (2) paracrystallinity g parameter.

(c) From absolute "wide-angle" peak intensities: (1) degree of crystallinity, (2) distortion factor (includes the Debye-Waller term), (3) carbon backbone setting angle.

(d) From "small-angle" peak positions: lamellar periodicity, lamellar thickness, and "amorphous" layer thickness (the latter two requiring the wide-angle degree of crystallinity data).

(e) From absolute integrated "small-angle" intensities: density of the interlamellar, "amorphous" layer.

The previous communications dealt entirely with polyethylene in the as-melt-crystallized state. The present paper extends the method to material strained *in situ* in the X-ray diffractometer.

The general purpose of the experimentation was to follow microstructural changes, primarily over the first 10% strain. In general, the microstructure of melt-crystallized polymers is spherulitic. Within the spherulite there is a tangential stacking of molecularly connected, alternating crystalline and amorphous layers, both having thicknesses of the order of 100 Å, but typically with the crystalline thickness some three times greater than the amorphous thickness. In such a system, one would intuitively expect the soft "amorphous" layer to accommodate the first several per cent of strain. When the elastic stress on the intercrystalline chains reaches some critical level, we would, again intuitively, expect the strain to possibly be accommodated by plastic flow in the crystalline regions. With this overview in mind it is convenient to proceed directly to the experimental procedure and results.

2. Experimental details

The material used was Marlex 6009, a linear polyethylene supplied by the Phillips Chemical Company. Specimens were compression moul-

*Present address: Mobil Research and Development Corporation, Paulsboro, New Jersey, USA.

TABLE I Preparative conditions

Specimen	Moulding Temperature	Time	Crystallization Temperature	Time
G–1	168–170°C	~ 5 min	123.0°C	26 h
G–2	155–160°C	~ 5 min	122.9°C	12 h
G–4	160–162°C	~ 5 min	123.0°C	18 h

ded as rectangular 1 mm thick plates. The specimens were transferred quickly while in the molten state, from the moulding press to a constant temperature bath at 123°C for isothermal crystallization. The preparative conditions for the three specimens reported are listed in Table I. Following crystallization, tensile specimens having a 1 to $1\frac{1}{2}$ in. gauge length and $\frac{3}{8}$ in. width were milled from the sheet.

The X-ray diffraction experiments were performed using the focusing diffractometer described previously [3]. In this apparatus, Cu K_α X-rays are monochromatized and focused to a line, using a ground and bent quartz crystal. The focused beam passes through the centre of a Picker biplane diffractometer and focuses on the arc describing the motion of the receiving slit of a scintillation counter. The specimen, set on the same arc, is placed in the path of the incident beam, forward of the diffractometer centre. This is just the diffractometer analogue of the symmetrical Guinier focusing camera. The specific usefulness of this instrument is that because of the focusing condition, it affords excellent resolution in both small-angle and wide-angle regimes and, because of the monochromatization, it permits of absolute intensity measurements, using calibrated attenuator foils.

For the present work, a new tensile deformation specimen holder was built. This device is shown in Fig. 1. Essentially, it is a small tensile tester. The specimen grips slide on four stainless steel rods. One set of grips is connected rigidly to a steel cantilever, for stress measurement. The other grips are moved by a micrometer screw, to set the strain level. The actual strain is measured on fiducial marks inked onto the specimen. The entire specimen-bearing device rotates up and out of the beam path. This latter feature is essential so that at each 2θ position both the "blank" beam and the beam with specimen in place may be measured; without such practice the small-angle signal cannot with precision be decoupled from instrumental background. The line of the beam (the effective slit) is normal to the draw direction. The detector traverses an arc which is essentially parallel to the draw direction near zero angle; i.e. our measurements are slit-smeared meridional scans.

The analysis of the wide-angle data was performed according to the procedure of Kavesh and Schultz [1]. In principle, the method operates as follows. The integrated intensity of the (hkl) reflection can be written

$$I_{hkl} = K_{hkl} \mid F_{hkl} \mid^2 D\phi, \qquad (1)$$

where K_{hkl} contains the Thomson constants and the usual geometrical and absorption terms for (hkl), F_{hkl} is the (hkl) structure factor, D is the

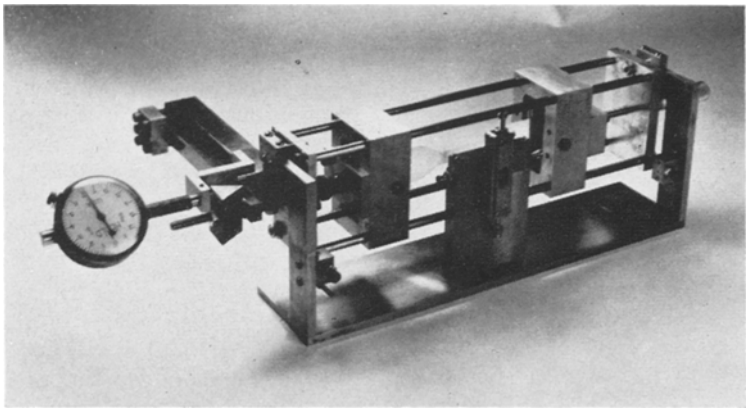

Figure 1 Tensile deformation apparatus for X-ray diffractometer.

distortion factor and includes the Debye-Waller term, and ϕ is the mass fraction of material within the boundaries of crystalline domains (the degree of crystallinity). In practice, the integrated intensity (above background and amorphous hump) of each (*hkl*) peak is measured. Then the several parameters of Equation 1 are fitted to these data to achieve a best fit. The fitting parameters are as follows. Due to the symmetry of the unit cell, and the assumed constancy of the C-H bonds, the structure factor is defined by two carbon atom position parameters x and y, as shown in Fig. 2. The distortion factor $D=\exp(-k_{ij}S_j^2)$ is separated into components $\exp(-k_\perp S_\perp^2)$ and $\exp(-k_\parallel S_\parallel^2)$ for S normal to and parallel to the chain axis. The fifth parameter to be fitted is the degree of crystallinity ϕ.

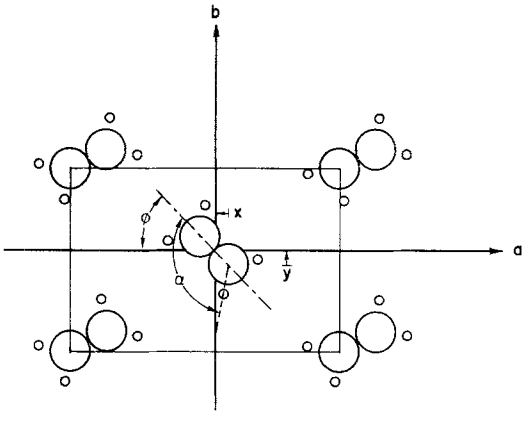

Figure 2 Polyethylene unit cell, viewed along the *c*-axis (chain axis).

The method of fitting the data is as described in [1], with one exception. This exception is that the contributions of the several integrated (*hkl*) reflections are here scaled proportionally to their areas in achieving the fit. This method reduces somewhat the problems associated with reading accurately the area under a low, broad peak.

The small angle (SAXS) data was analysed according to the procedure in [2]. Broadly, what is done here is to determine the positions of "Bragg" humps and to also measure the integrated small angle intensity. The positions of the Bragg humps relate to the spacing of the stacked lamellae. The integrated intensity is written, for a slit-collimated incident beam,

$$\int_0^\infty S\frac{I(S)}{I_e(S)}\,dS = V(\rho_c-\rho_a)^2\phi(1-\phi), \quad (2)$$

where $S=2\sin\theta/\lambda$, $I(S)$ is the measured intensity, $I_e(S)$ is the Thomson intensity, V is the irradiated specimen volume, ρ_c and ρ_a are the crystalline and amorphous phase electron densities, and ϕ again is the degree of crystallinity. Clearly, when ϕ is found via Equation 1 and ρ_c is obtained from the unit cell parameters, ρ_a may be extracted from Equation 2.

For the analysis of both Equations 1 and 2 it is necessary to perform absolute intensity measurements. In principle this can be done using calibrated beam attenuators and we have made measurements using such attenuators. However, due to uncertainties in the atomic scattering factor for carbon at the low angles of polyethylene crystalline diffraction, the absolute intensities measured directly appear to be too high. The intensity data were therefore scaled according to the diffraction intensity of crystalline peaks in a very highly crystalline, pressure-crystallized sample supplied by R. B. Prime and B. Wunderlich. For the procedure, again see [1].

3. Results

3.1. From wide-angle diffraction

According to the fitting procedure outlined above, the analysis of wide-angle line intensities must yield values of the degree of crystallinity ϕ; the carbon atom position parameters x,y; and the distortion factor D. We report here only the crystallinity and position results; there was little systematic change in D during this set of experiments.

Somewhat surprisingly, the degree of crystallinity was observed to decrease with increasing strain. This effect is shown in Fig. 3. This general feature is observed in all three specimens studied.

For atomic position parameters x,y as derived via best fit, it is observed that y decreases with increasing strain. The trend for x is not so clear cut, but it appears that x changes more slowly with strain than does y. The angle ψ between the carbon backbone and the *ac* plane is related to x,y through $\psi = \arctan y/x$ (see Fig. 2). This "setting angle" is plotted against strain in Fig. 4. The trend in ψ is generally for it to decrease with increasing ϵ.

3.2. From small-angle scattering

Small-angle (SAXS) data was recorded for only two of the three specimens. As in the previous work [1, 2], two humps could be observed in

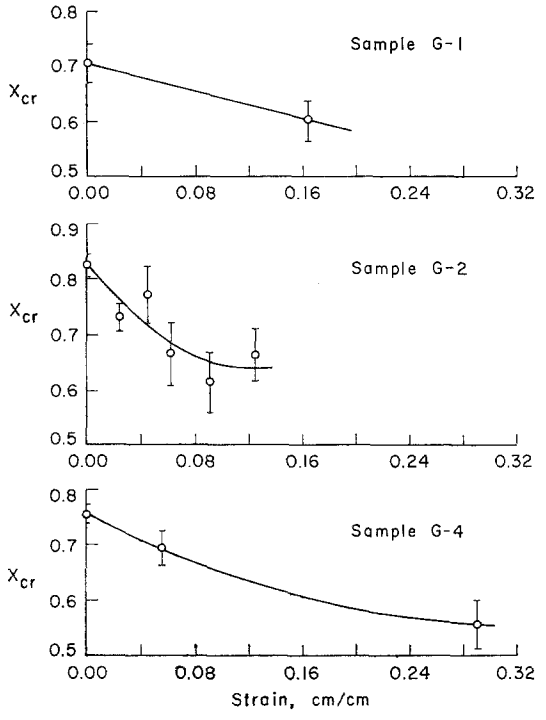

Figure 3 Effect of strain on volume fraction crystallinity.

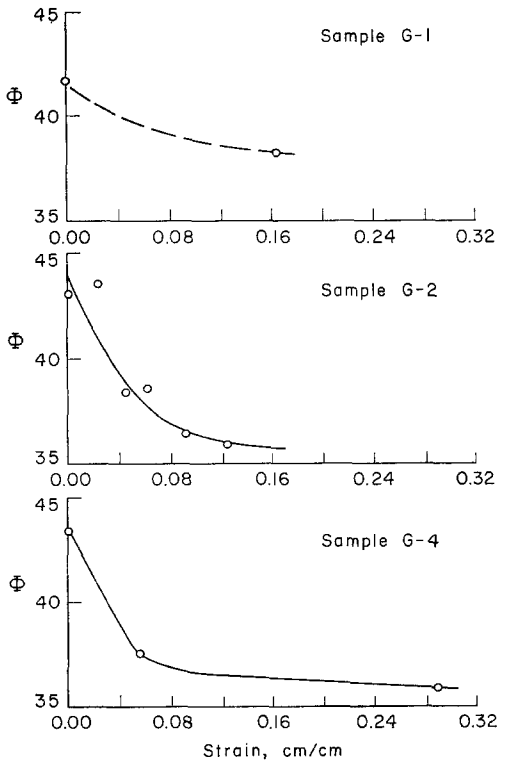

Figure 4 Effect of strain on the setting angle (angle between molecular plane and *ac* lattice plane).

the raw, slit-smeared SAXS traces. These humps resolved as peaks when the data was desmeared. The long period P obtained from the desmeared curves is shown in Fig. 5. Values of P for both peaks are shown there. The general trend is for l to increase with the strain ϵ.

As we reported previously, the two long periods appear to be first and second orders representing the same periodicity. The data on which this result is based in the present work is shown in Fig. 6. Here the ratio P_1:P_2 of the two long spacings is shown against strain. For the slit-corrected data, this ratio always lies between 2 and 2.5, in satisfactory agreement with the expected ratio of 2.0. Note that the uncorrected data yields values of P_1:P_2 which lie far from 2:1.

Using the results relating to the degree of crystallinity and the long period, the thickness l and t of the lamellar and interlamellar (amorphous) layers were computed from a mass balance:

$$\phi P_1 = l \qquad (3)$$
$$(1 - \phi)P_1 = t\,.$$

These results are shown as Fig. 7. It is seen that the lamellar thickness continuously decreases and that the interlamellar thickness continuously increases with strain.

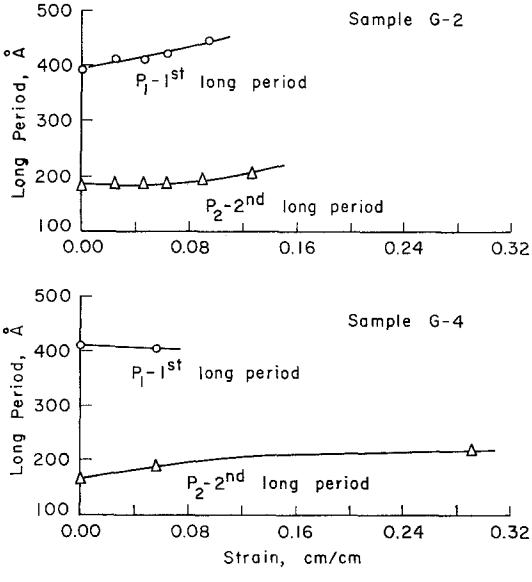

Figure 5 Effect of strain on meridional long period.

The SAXS results of Figs. 5-7 depend on an explicit model of the microstructure – i.e. a

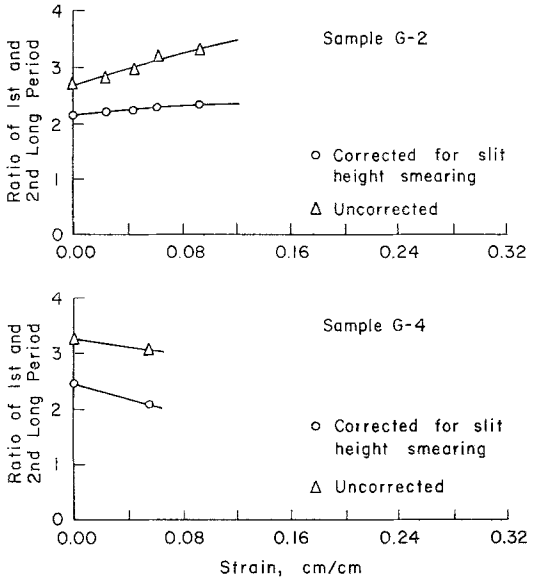

Figure 6 Ratio of long periods.

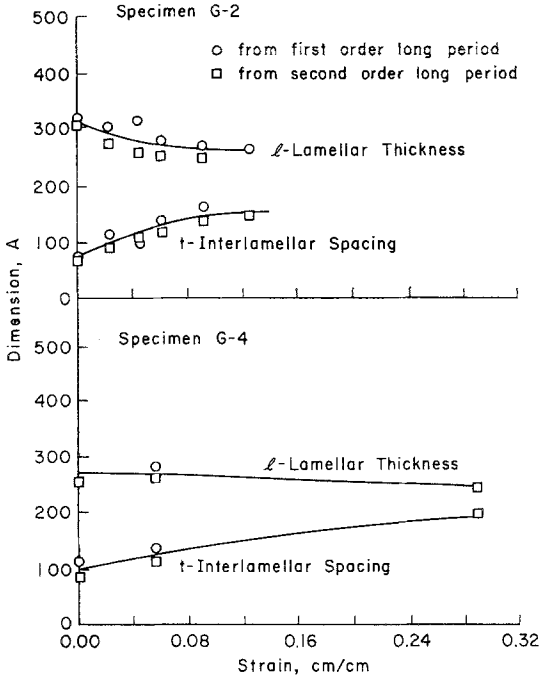

Figure 7 Effect of strain on lamellar and "amorphous layer" thicknesses, along the tensile direction

periodic stacking of lamellae separated by amorphous interlamellar zones. These results are then potentially reliable only to the extent to which the model is accurate. And that cannot be assessed fully at present. The reason for mentioning the model dependence at this point, is to put into context the relative model independence of the amorphous density ρ_a found via Equation 2. This relationship is derived with essentially only one significant assumption regarding the model. That presupposition is that only two homogeneous phases are present and that a sharp boundary exists between these two. While this is still a stringent restriction, it is much less so than the assumptions leading to the statement of the other SAXS results.

The amorphous density, plotted against strain, is shown in Fig. 8. Here, the amorphous density initially rises rapidly with strain and then finally levels off. The variation in the initial values of ρ_a are presumably due to differences in the processing conditions (see Table I), although the exact genesis of the differences is not an obvious one.

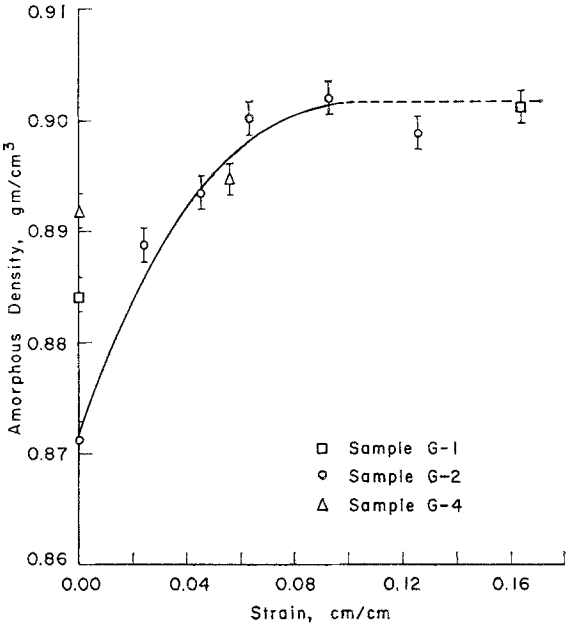

Figure 8 Variation of density of the amorphous layer with strain.

4. Discussion

Before proceeding to a discussion of the results themselves, it is necessary to look at the effect of errors due to orientation effects. It has been shown that at some sufficiently high strain the small- and wide-angle X-ray patterns of semicrystalline polymers develop a texture, due to preferred orientation of the crystallites [4-7]. For linear polyethylene deformed at room tem-

perature, the critical strain level appears to be near 20% [4, 5]. Indeed, pinhole wide-angle X-ray patterns from our tensile specimens show no visible orientation until a strain of some 20 to 24% has been reached. In this context, then, we should expect the results for our lowest strain levels to be nearly quantitatively correct, whereas the results from strain levels above 20% can at best only indicate a direction. With this restraint in mind, we now proceed to interpret the results.

The general trend of results is summarized here.

(1) The setting angle of the carbon backbone decreases with strain.
(2) The degree of crystallinity decreases with strain.
(3) The long period increases with strain.
(4) The lamellar thickness increases and the interlamellar thickness decreases with strain.

These results can be explained on the following model. As the elastic strain increases, the unit cell deforms. As the cell is deformed, the backbone rotates to maintain the optimal hydrogen-hydrogen distance. Simultaneously some interlamellar tie chains are extended, and these accommodate the bulk of the macroscopic strain. The long period increase which has also been observed by others [6-12] and the increase in interlamellar thickness are consistent with this interpretation. Since our slit traverses an arc essentially parallel to the draw direction, this result will pertain to the lamellae which lie normal or nearly normal to the draw direction. The decrease in crystallinity is less easily explained.

We see that two possibilities exist.

(1) Some lamellar strands which are attached directly to intercrystalline tie chains are pulled out of the crystal.
(2) Condensed interlamellar linkage similar to, but smaller than, those observed by Vadimsky *et al* [13] are destroyed, presumably because of a very high strain on the shortest strands of the links.

Both of these possibilities are consistent with the observations. The second explanation, however, would need interlamellar crystallites to be included in the microstructural model and would largely obviate quantitative conclusions from these data.

The destruction of crystallites as an element of the instability leading to yielding (or necking) has been suggested [14-16], but crystallite destruction in the elastic region preceding necking is a new observation. It is hoped that this observation might stimulate further exploration of the prenecking elastic region.

5. Summary

"Absolute intensity" wide- and small-angle experiments were performed on melt-crystallized polyethylene as it underwent tensile deformation in the X-ray diffractometer. The data were analysed according to a scheme set down previously. The results showed that as the strain was increased to some 8 to 12%, the carbon backbone rotated toward the *ac*-plane, the interlamellar thickness increased, the crystallites thinned somewhat, and the degree of crystallinity increased. Beyond this level of strain little change was observed in these parameters. It is concluded that the interlamellar, non-crystalline layer contributes significantly to deformation below that critical strain. Above this level intracrystalline processes must dominate.

Acknowledgement

This work was supported by the National Science Foundation.

References

1. S. KAVESH and J. M. SCHULTZ, *J. Polymer Sci.* **8A-2** (1970) 243.
2. *Idem, ibid* **9A-2** (1971) 85.
3. *Idem, Rev. Sci. Inst.* **40** (1969) 98.
4. A. BROWN, *J. Polymer Sci.* **20** (1949) 552.
5. R. S. STEIN and F. A. NORRIS, *ibid* **21** (1956) 381.
6. N. KASAI, M. KAKUDO, and T. WATASE, *Kogyo Kagaku Zasshi*, **59** (1956) 786.
7. R. J. SAMUELS, *J. Polymer Sci.* **20C** (1967) 253.
8. H. HENDUS, *Kolloid-Z.* **165** (1959) 32.
9. N. KASAI and M. KAKUDO, *J. Polymer Sci.* **2A** (1964) 1955.
10. S. N. ZHURKOV, A. I. SLUTSKER, and A. A. YASTREBINSKI, *Sov. Phys., Solid State* **6** (1965) 2881.
11. K. ISHIKAWA, K. MIYASIKA, M. MAEDA, and M. YAMADA, *J. Polymer Sci.* **7A-2** (1969) 1259.
12. A. PETERLIN and G. MEINEL, *Makromol. Chem.* **142** (1971) 227.
13. H. D. KEITH, F. J. PADDEN, JUN., and R. G. VADIMSKY, *Science* **150** (1965) 1026; *J. Polymer Sci.* **4A-2** (1966) 267; *J. Appl. Phys.* **37** (1966) 4027.
14. A. PETERLIN, *J. Polymer Sci.* **15C** (1966) 185.
15. E. J. KRAMER, *J. Appl. Phys.* **41** (1970) 4327.
16. Y. WADA and A. NAKAYAMA, *J. Appl. Polymer Sci.* **15** (1971) 183.

Received 10 April and accepted 14 June 1972.